PHYSICAL REVIEW D **76,** 012006 (2007)

Study of $\bar{B}^0 \to D^0\pi^+\pi^-$ decays

A. Kuzmin,[1] K. Abe,[8] I. Adachi,[8] H. Aihara,[45] D. Anipko,[1] K. Arinstein,[1] V. Aulchenko,[1] T. Aushev,[13,18] S. Bahinipati,[4] A. M. Bakich,[40] V. Balagura,[13] E. Barberio,[21] M. Barbero,[7] A. Bay,[18] I. Bedny,[1] K. Belous,[12] U. Bitenc,[14] I. Bizjak,[14] S. Blyth,[24] A. Bondar,[1] A. Bozek,[27] M. Bračko,[8,14,20] T. E. Browder,[7] M.-C. Chang,[5] Y. Chao,[26] A. Chen,[24] K.-F. Chen,[26] W. T. Chen,[24] B. G. Cheon,[3] R. Chistov,[13] Y. Choi,[39] Y. K. Choi,[39] J. Dalseno,[21] M. Dash,[49] A. Drutskoy,[4] S. Eidelman,[1] D. Epifanov,[1] N. Gabyshev,[1] A. Garmash,[51] T. Gershon,[8] A. Go,[24] G. Gokhroo,[41] B. Golob,[14,19] H. Ha,[16] J. Haba,[8] K. Hayasaka,[22] H. Hayashii,[23] M. Hazumi,[8] D. Heffernan,[32] T. Hokuue,[22] Y. Hoshi,[43] S. Hou,[24] W.-S. Hou,[26] Y. B. Hsiung,[26] T. Iijima,[22] K. Ikado,[22] A. Imoto,[23] K. Inami,[22] A. Ishikawa,[45] H. Ishino,[46] R. Itoh,[8] M. Iwasaki,[45] Y. Iwasaki,[8] J. H. Kang,[50] P. Kapusta,[27] H. Kawai,[2] T. Kawasaki,[29] H. Kichimi,[8] H. J. Kim,[17] Y. J. Kim,[6] K. Kinoshita,[4] P. Križan,[14,19] P. Krokovny,[8] R. Kulasiri,[4] R. Kumar,[33] C. C. Kuo,[24] Y.-J. Kwon,[50] S. E. Lee,[37] T. Lesiak,[27] S.-W. Lin,[26] G. Majumder,[41] F. Mandl,[11] T. Matsumoto,[47] S. McOnie,[40] W. Mitaroff,[11] K. Miyabayashi,[23] H. Miyake,[32] H. Miyata,[29] Y. Miyazaki,[22] R. Mizuk,[13] G. R. Moloney,[21] Y. Nagasaka,[9] E. Nakano,[31] M. Nakao,[8] Z. Natkaniec,[27] S. Nishida,[8] O. Nitoh,[48] S. Noguchi,[23] T. Ohshima,[22] S. Okuno,[15] S. L. Olsen,[7] Y. Onuki,[35] P. Pakhlov,[13] G. Pakhlova,[13] H. Park,[17] L. S. Peak,[40] R. Pestotnik,[14] L. E. Piilonen,[49] A. Poluektov,[1] H. Sahoo,[7] Y. Sakai,[8] N. Satoyama,[38] T. Schietinger,[18] O. Schneider,[18] J. Schümann,[25] C. Schwanda,[11] A. J. Schwartz,[4] K. Senyo,[22] M. Shapkin,[12] H. Shibuya,[42] B. Shwartz,[1] V. Sidorov,[1] A. Sokolov,[12] A. Somov,[4] S. Stanič,[30] M. Starič,[14] H. Stoeck,[40] K. Sumisawa,[8] T. Sumiyoshi,[47] S. Y. Suzuki,[8] F. Takasaki,[8] K. Tamai,[8] N. Tamura,[29] M. Tanaka,[8] G. N. Taylor,[21] Y. Teramoto,[31] X. C. Tian,[34] K. Trabelsi,[7] T. Tsuboyama,[8] T. Tsukamoto,[8] S. Uehara,[8] T. Uglov,[13] K. Ueno,[26] Y. Unno,[3] S. Uno,[8] P. Urquijo,[21] Y. Usov,[1] G. Varner,[7] K. E. Varvell,[40] S. Villa,[18] C. H. Wang,[25] M.-Z. Wang,[26] Y. Watanabe,[46] E. Won,[16] C.-H. Wu,[26] Q. L. Xie,[10] B. D. Yabsley,[40] A. Yamaguchi,[44] Y. Yamashita,[28] M. Yamauchi,[8] L. M. Zhang,[36] Z. P. Zhang,[36] V. Zhilich,[1] and A. Zupanc[14]

(Belle Collaboration)

[1]*Budker Institute of Nuclear Physics, Novosibirsk*
[2]*Chiba University, Chiba*
[3]*Chonnam National University, Kwangju*
[4]*University of Cincinnati, Cincinnati, Ohio 45221*
[5]*Department of Physics, Fu Jen Catholic University, Taipei*
[6]*The Graduate University for Advanced Studies, Hayama, Japan*
[7]*University of Hawaii, Honolulu, Hawaii 96822*
[8]*High Energy Accelerator Research Organization (KEK), Tsukuba*
[9]*Hiroshima Institute of Technology, Hiroshima*
[10]*Institute of High Energy Physics, Chinese Academy of Sciences, Beijing*
[11]*Institute of High Energy Physics, Vienna*
[12]*Institute of High Energy Physics, Protvino*
[13]*Institute for Theoretical and Experimental Physics, Moscow*
[14]*J. Stefan Institute, Ljubljana*
[15]*Kanagawa University, Yokohama*
[16]*Korea University, Seoul*
[17]*Kyungpook National University, Taegu*
[18]*Swiss Federal Institute of Technology of Lausanne, EPFL, Lausanne*
[19]*University of Ljubljana, Ljubljana*
[20]*University of Maribor, Maribor*
[21]*University of Melbourne, Victoria*
[22]*Nagoya University, Nagoya*
[23]*Nara Women's University, Nara*
[24]*National Central University, Chung-li*
[25]*National United University, Miao Li*
[26]*Department of Physics, National Taiwan University, Taipei*
[27]*H. Niewodniczanski Institute of Nuclear Physics, Krakow*
[28]*Nippon Dental University, Niigata*
[29]*Niigata University, Niigata*
[30]*University of Nova Gorica, Nova Gorica*
[31]*Osaka City University, Osaka*

[32]*Osaka University, Osaka*
[33]*Panjab University, Chandigarh*
[34]*Peking University, Beijing*
[35]*RIKEN BNL Research Center, Upton, New York 11973*
[36]*University of Science and Technology of China, Hefei*
[37]*Seoul National University, Seoul*
[38]*Shinshu University, Nagano*
[39]*Sungkyunkwan University, Suwon*
[40]*University of Sydney, Sydney NSW*
[41]*Tata Institute of Fundamental Research, Bombay*
[42]*Toho University, Funabashi*
[43]*Tohoku Gakuin University, Tagajo*
[44]*Tohoku University, Sendai*
[45]*Department of Physics, University of Tokyo, Tokyo*
[46]*Tokyo Institute of Technology, Tokyo*
[47]*Tokyo Metropolitan University, Tokyo*
[48]*Tokyo University of Agriculture and Technology, Tokyo*
[49]*Virginia Polytechnic Institute and State University, Blacksburg, Virginia 24061*
[50]*Yonsei University, Seoul*
[51]*Princeton University, Princeton, New Jersey 08544*
(Received 29 November 2006; published 30 July 2007)

We report the results of a study of neutral B meson decays to the $D^0\pi^+\pi^-$ final state, where the D^0 is fully reconstructed. The results are obtained from an event sample containing 388×10^6 $B\bar{B}$-meson pairs collected in the Belle experiment at the KEKB e^+e^- collider. The total branching fraction of the three-body decay $\mathcal{B}(\bar{B}^0 \to D^0\pi^+\pi^-) = (8.4 \pm 0.4(\text{stat}) \pm 0.8(\text{syst})) \times 10^{-4}$ has been measured. The intermediate resonant structure of these three-body decays has been studied. From a Dalitz plot analysis we have obtained the product of the branching fractions for D_2^{*+} and D_0^{*+} production: $\mathcal{B}(\bar{B}^0 \to D_2^{*+}\pi^-) \times \mathcal{B}(D_2^{*+} \to D^0\pi^+) = (2.15 \pm 0.17(\text{stat}) \pm 0.29(\text{syst}) \pm 0.12(\text{mod})) \times 10^{-4}$, and $\mathcal{B}(\bar{B}^0 \to D_0^{*+}\pi^-) \times \mathcal{B}(D_0^{*+} \to D^0\pi^+) = (0.60 \pm 0.13(\text{stat}) \pm 0.15(\text{syst}) \pm 0.22(\text{mod})) \times 10^{-4}$. This is the first observation of the $\bar{B}^0 \to D_0^{*+}\pi^-$ decay. The $\bar{B}^0 \to D^0\rho^0$ and $D^0 f_2$ branching fractions are measured to be: $\mathcal{B}(\bar{B}^0 \to D^0\rho^0) = (3.19 \pm 0.20(\text{stat}) \pm 0.24(\text{syst}) \pm 0.38(\text{mod})) \times 10^{-4}$, and $\mathcal{B}(\bar{B}^0 \to D^0 f_2) = (1.20 \pm 0.18(\text{stat}) \pm 0.21(\text{syst}) \pm 0.32(\text{mod})) \times 10^{-4}$.

DOI: 10.1103/PhysRevD.76.012006 PACS numbers: 13.25.Hw, 14.40.Lb, 14.40.Nd

I. INTRODUCTION

The decay $\bar{B}^0 \to D^0\pi^+\pi^-$ includes intermediate states $D^{**+}\pi^-$, where D^{**}'s are P-wave excitations of states containing one charmed and one light ($q = u, d$) quark that decay to the $D^0\pi^+$ final state. Figure 1 shows the spectrum and the allowed transitions of $c\bar{q}$-meson states. In the heavy-quark limit, the c-quark spin $\vec{s}_c$ decouples from the other degrees of freedom, and the total angular momentum of the light quark which is the sum of orbital momentum ($\vec{L}$) and light quark spin ($\vec{s}_q$) $\vec{j}_q = \vec{L} + \vec{s}_q$ is a good quantum number. Four P-wave states with the quantum numbers (J^P): $0^+(j_q = 1/2)$, $1^+(j_q = 1/2)$, $1^+(j_q = 3/2)$, and $2^+(j_q = 3/2)$ are expected; these are usually labeled as D_0^*, D_1', D_1, and D_2^*, respectively.

The two $j_q = 3/2$ states have narrow widths of about 20–40 MeV and are well established [1–11]. The measured masses agree with model predictions [12–15]. The remaining $j_q = 1/2$ states are expected to be broad and decay via S waves. The $B \to D\pi\pi$ decay process provides a way to study D^{**} production. Angular analysis of the decay products can be used to determine D^{**} meson quantum numbers. These results also provide a test of heavy-quark effective theory (HQET) and QCD sum rules [16,17].

A study of neutral D^{**0} production in charged B-decays has been recently reported by Belle [18], where four D^{**} states are observed and the production rates of the broad ($j = 1/2$) states are found to be of the same order of magnitude as those for the narrow ($j = 3/2$) states. This

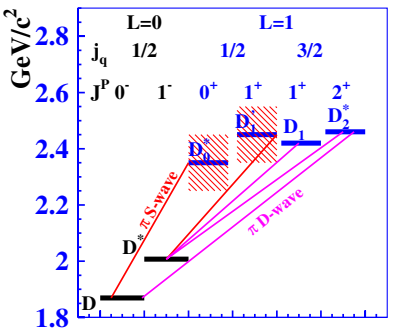

FIG. 1 (color online). Spectrum of $c\bar{q}$-meson excitations. The lines indicate possible one-pion transitions. The D_0^*, D_1' mesons are broad which is indicated by shaded areas.

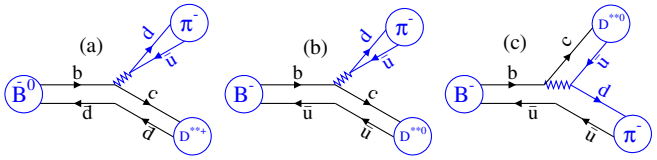

FIG. 2 (color online). Quark-line diagrams for neutral (a) and charged (b and c) B decays.

paper describes an analysis of the $\bar{B}^0 \to D^0\pi^+\pi^-$ decay that is performed in a manner similar to that of the previous Belle analysis of the $\bar{B}^0 \to D^{**+}\pi^-$ decay [19]. The results presented here supersede those of Ref. [19].

The neutral B decay to $D^{**}\pi$ is described only by the tree diagram shown in Fig. 2(a) while for the charged B decay to $D^{**}\pi$, the amplitude receives contributions from both a tree and a color-suppressed diagram as shown in Fig. 2(b) and 2(c).

D^{**} tree-diagram production amplitudes are described by the Isgur-Wise functions $\tau_{1/2}$ and $\tau_{3/2}$. According to a QCD sum rule [16,17], $\tau_{1/2} \ll \tau_{3/2}$ and one would expect suppression of decays to the broad state. The observation that the production rates of the broad ($j = 1/2$) states are comparable with those of the narrow ($j = 3/2$) states indicates either a large contribution of the color-suppressed diagram or the violation of the sum rule. Measurement of the decay rates of the neutral B allows one to test the contribution of the tree-diagram only and also test the QCD sum rule.

In this analysis, the final state contains two pions of opposite sign, and these can originate from resonant states such as the ρ^0, f_0, f_2, etc. While the possible presence of $\pi\pi$ resonant structures complicates the analysis, it also provides useful information about the mechanism of these decays.

II. THE BELLE DETECTOR

The Belle detector [20] is a large-solid-angle magnetic spectrometer that consists of a silicon vertex detector (SVD), a 50-layer central drift chamber (CDC) for charged particle tracking and specific ionization measurement (dE/dx), an array of aerogel threshold Čerenkov counters (ACC), time-of-flight scintillation counters (TOF), and an array of 8736 CsI(Tl) crystals for electromagnetic calorimetry (ECL) located inside a superconducting solenoid coil that provides a 1.5 T magnetic field. An iron flux return (KLM) located outside the coil is instrumented to detect K_L^0 mesons and identify muons. We use a GEANT-based Monte Carlo (MC) simulation to model the response of the detector and determine its acceptance [21].

Separation of kaons and pions is accomplished by combining the responses of the ACC and the TOF with dE/dx measurements in the CDC to form a likelihood $\mathcal{L}(h)$ where $h = (\pi)$ or (K). Charged particles are identified as pions or kaons using the likelihood ratio ($\mathcal{R}$):

$$\mathcal{R}(K) = \frac{\mathcal{L}(K)}{\mathcal{L}(K) + \mathcal{L}(\pi)};$$

$$\mathcal{R}(\pi) = \frac{\mathcal{L}(\pi)}{\mathcal{L}(K) + \mathcal{L}(\pi)} = 1 - \mathcal{R}(K).$$

A more detailed description of the Belle particle identification can be found in Ref. [22].

III. EVENT SELECTION

A data sample of 357 fb^{-1} (388×10^6 $B\bar{B}$ events) collected at the $\Upsilon(4S)$ resonance is used in this analysis. Candidate $\bar{B}^0 \to D^0\pi^+\pi^-$ events are selected, where the D^0 mesons decay via the $D^0 \to K^-\pi^+$ mode. The signal-to-noise ratios for other D^0 decay modes are found to be significantly lower and, therefore, these are not used. (The inclusion of charge conjugate states is implied by default throughout this paper.)

Charged tracks are selected with requirements based on the average hit residuals and impact parameters relative to the interaction point. We require that the polar angle of each track be in the angular range of 17°–150° and that the track transverse momentum be greater than 50 MeV/c.

Charged kaon candidates are identified by the requirement $\mathcal{R}(K) > 0.6$, which has an efficiency of 90% and a pion misidentification probability of approximately 10%. For pion candidates we require $\mathcal{R}(\pi) > 0.2$. Kaon and pion candidates are rejected if the track is positively identified as an electron.

Candidate D^0 mesons are $K^-\pi^+$ combinations with an invariant mass within ± 12 MeV/c^2 of the nominal D^0 mass, which corresponds to $\sim 2.5\sigma_{K\pi}$. We reject D^0 candidates that, when combined with any π^0 in the event, has a value of $M_{D\pi^0} - M_{D^0}$ that is within ± 2.5 MeV/c^2 of the nominal $D^{*0} - D^0$ mass difference.

B meson candidates are identified by their center-of-mass (c.m.) energy difference $\Delta E = (\sum_i E_i) - E_{\rm b}$, and the beam-constrained mass $M_{\rm bc} = \sqrt{E_{\rm b}^2 - (\sum_i \vec{p}_i)^2}$, where $E_{\rm b} = \sqrt{s}/2$ is the beam energy in the $\Upsilon(4S)$ c.m. frame, and $\vec{p}_i$ and E_i are the c.m. three-momenta and energies, respectively, of the B meson candidate decay products. We select events satisfying $M_{\rm bc} > 5.25$ GeV/c^2 and $|\Delta E| < 0.10$ GeV.

To suppress the large continuum background ($e^+e^- \to q\bar{q}$, where $q = u, d, s, c$), topological variables are used. Since the produced B mesons are almost at rest in the c.m. frame, the signal-event shapes tend to be isotropic while continuum $q\bar{q}$ events tend to have a two-jet structure. We use the angle between the thrust axis of the B candidate and that of the rest of the event ($\Theta_{\rm thrust}$) to discriminate between these two cases. The distribution of $|\cos\Theta_{\rm thrust}|$ is strongly peaked near $|\cos\Theta_{\rm thrust}| = 1$ for $q\bar{q}$ events and is nearly flat for $\Upsilon(4S) \to B\bar{B}$ events. We require $|\cos\Theta_{\rm thrust}| < 0.8$, which eliminates about 83% of the continuum background while retaining about 80% of signal events.

There are events for which two or more track combinations pass all the selection criteria. According to MC simulation, this occurs primarily because of the misreconstruction of the low momentum pion from $D^{**} \to D\pi$ decays. To avoid multiple entries, the combination that has the minimum difference of z coordinates at the interaction point, $|z_{\pi_1} - z_{\pi_2}|$, of the tracks corresponding to the pions from $B \to D\pi_1\pi_2$ are selected [23]. This selection also suppresses combinations that include pions from K^0_S decays. In the case of multiple $D \to K\pi$ combinations, the one with the invariant mass closest to the D^0 mass is selected.

IV. $\bar{B}^0 \to D^0\pi^+\pi^-$ BRANCHING FRACTION

The $D^0\pi^+\pi^-$ final state, together with three-body and quasi-two-body contributions, includes the two-body $\bar{B}^0 \to D^{*+}\pi^-$ decay followed by the decay $D^{*+} \to D^0\pi^+$. We obtain the branching fraction of the three-body decay $\bar{B}^0 \to D^0\pi^+\pi^-$ excluding the contribution of $\bar{B}^0 \to D^{*+}\pi^-$. Using the $M_{D\pi} - M_D$ mass difference, we subdivide the total sample into two subsamples as follows. Events that have a $D\pi$ combination with $M_{D\pi} - M_D$ within 3 MeV/c^2 ($\sim 6\sigma$) of the nominal $D^{*+} - D^0$ mass difference are denoted below as sample (2); the rest of the $D\pi\pi$ events are denoted as sample (1). Sample (2) is used to crosscheck our procedures.

The $M_{\rm bc}$ and ΔE distributions for $\bar{B}^0 \to D^0\pi^+\pi^-$ events are shown in Fig. 3. The distributions are plotted for events that satisfy the selection criteria for the other variable: $|\Delta E| < 25$ MeV and $|M_{\rm bc} - m_B| < 7$ MeV/c^2 for the $M_{\rm bc}$ and ΔE histograms, respectively, where m_B is the nominal B mass. Distinct signals are evident in all of the distributions.

The background shape is obtained from generic MC data samples that include B^+B^- (BC) and $B^0\bar{B}^0$ (BN), continuum charm production (CC), and continuum with light quarks (UDS), each corresponding to approximately twice the luminosity of the experimental data. The $D\pi$ and $\pi\pi$ invariant mass distributions are different for different MC samples. The branching fractions used in the generic MC are measured with some experimental uncertainty and may not reproduce the experimental data. To improve the quality of the MC spectra, relative weights of these four components are determined from a fit to a two-dimensional Dalitz plot ($q^2 \equiv M^2_{D\pi}$ [24] vs $q^2_1 \equiv M^2_{\pi\pi}$) distribution for events in the ΔE sideband shown in Fig. 4. The fitting function represents the sum of the four two-dimensional

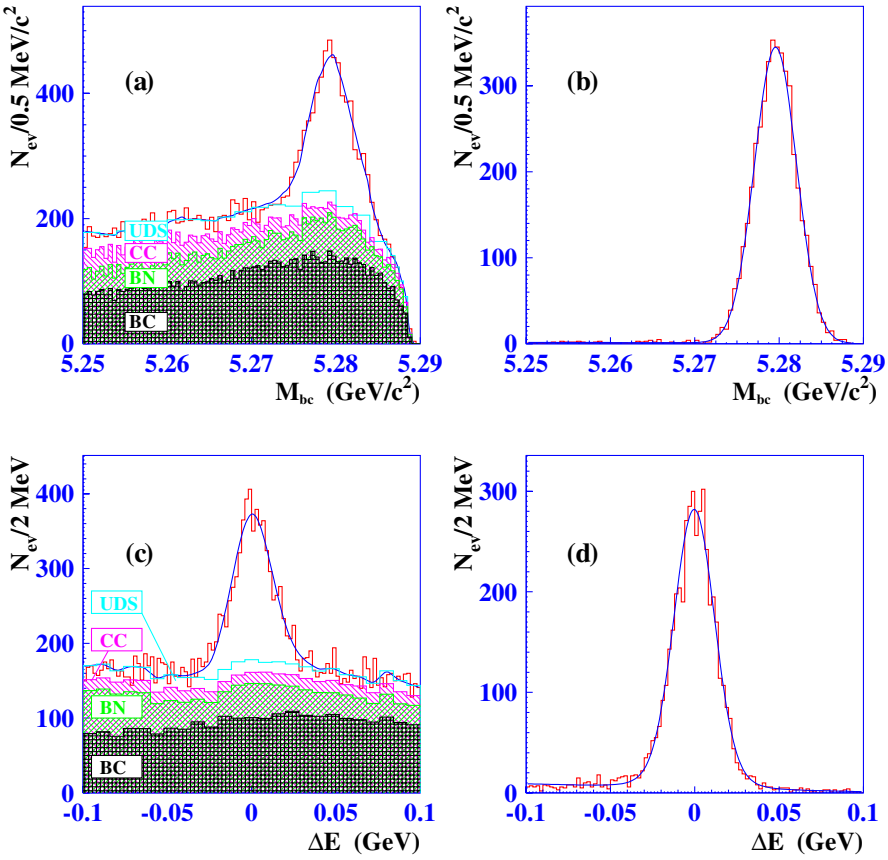

FIG. 3 (color online). $M_{\rm bc}$ and ΔE distributions for $\bar{B}^0 \to D^0\pi^+\pi^-$ events. Sample (1) distributions are shown in (a) and (c); those for sample (2) are shown in (b) and (d).

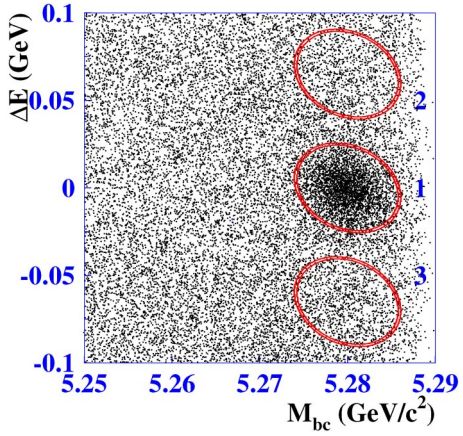

FIG. 4 (color online). The experimental distribution in the ($M_{\rm bc}$-ΔE) plane. The ellipses show the signal (1) and sideband regions (2 and 3).

histograms with floating weights. Each histogram is determined from its respective MC sample. The weights obtained for the four components are: $a_{\rm BC} = 1.10 \pm 0.07$, $a_{\rm BN} = 1.37 \pm 0.22$, $a_{\rm CC} = 0.52 \pm 0.12$, $a_{\rm UDS} = 0.92 \pm 0.22$. The ΔE background shape is described as $F_{\rm bg}(\Delta E) = \sum_i a_i F_i(\Delta E)$, where $F_i(\Delta E)$ is the ΔE distribution of the ith component obtained from the MC sample.

The signal yield is obtained by fitting the ΔE distribution to the sum of two Gaussians with the same mean value to describe the signal, plus the above-described background function $F_{\rm bg}(\Delta E)$. The width of the broader Gaussian and the relative normalization of the two Gaussians are fixed to the values obtained from a MC simulation; the signal and background normalization as well as the width of the narrow Gaussian are left as free parameters.

The fitted signal yields are 2909 ± 115 events and 4202 ± 67 events for samples (1) and (2), respectively. The reconstruction efficiencies $(23.4 \pm 0.4)\%$ and $(19.0 \pm 0.4)\%$ are determined from a MC simulation that uses a Dalitz plot distribution that is generated according to the model described in the next section. Taking into account $\mathcal{B}(D^0 \to K^-\pi^+) = (3.80 \pm 0.07)\%$ [25], we obtain the following branching fraction:

$$\mathcal{B}(\bar{B}^0 \to D^0\pi^+\pi^-) = (8.4 \pm 0.4 \pm 0.8) \times 10^{-4},$$

where the first error is statistical and second error is systematic. Various contributions to the systematic error are listed in Table I for both samples. They include tracking efficiency, particle identification efficiency, limited MC statistics, and background uncertainty. To estimate the background uncertainty we performed a fit of the signal data Dalitz plot for four different methods of describing background with weights of the separate components set to: unity, the results of the fit of the data in both sidebands; and left and right sideband separately. The obtained differences are included in the systematic uncertainty. We also varied the relative weights of MC within their errors. The contribution of the nonresonant $\bar{B}^0 \to K^-\pi^+\pi^-\pi^+$ is estimated using the $K\pi$ mass sidebands of the D mass region and is negligible.

TABLE I. The systematic uncertainties for the $\bar{B}^0 \to D^0\pi^+\pi^-$ branching fraction measurement.

	Sample (1)	Sample (2)
Particle identification	5%	5%
Background uncertainty	5%	1%
Tracking efficiency	4.4%	5.4%
MC statistics	3%	3%
$\mathcal{B}(D, D^*)$ uncertainty	2.4%	2.5%
Total	9.2%	8.1%

The value of $\mathcal{B}(\bar{B}^0 \to D^0\pi^+\pi^-)$ improves and supersedes the previous Belle result $\mathcal{B}(\bar{B}^0 \to D^0\pi^+\pi^-) = (8.0 \pm 1.6) \times 10^{-4}$ [26]. The value of the branching fraction $\mathcal{B}(\bar{B}^0 \to D^{*+}\pi^-)$ is obtained using sample (2) and the PDG value $\mathcal{B}(D^{*+} \to D^0\pi^+) = (67.7 \pm 0.5)\%$ [25]. The result is $\mathcal{B}(\bar{B}^0 \to D^{*+}\pi^-) = (2.22 \pm 0.04 \pm 0.19) \times 10^{-3}$, which is somewhere lower than the CLEO result $\mathcal{B}(\bar{B}^0 \to D^{*+}\pi^-) = (2.81 \pm 0.25) \times 10^{-3}$ [27].

A. $B \to D\pi\pi$ Dalitz plot analysis

For the decay of a spin zero state to three spinless particles, two variables are required to describe the decay kinematics; we use the $D^0\pi^+$ and $\pi^+\pi^-$ invariant masses squared, $M^2_{D\pi}$ and $M^2_{\pi\pi}$, respectively.

To analyze the dynamics of $B \to D\pi\pi$ decays, sample (1) events with ΔE and $M_{\rm bc}$ within the signal region $((\Delta E + \kappa(M_{\rm bc} - m_B))/\sigma_{\Delta E})^2 + ((M_{\rm bc} - m_B)/\sigma_{M_{\rm bc}})^2 < 4$ are selected. The parameters $\sigma_{\Delta E} = 11$ MeV, $\sigma_{M_{\rm bc}} = 2.7$ MeV/c^2, and $\kappa = 0.9$ are determined from a fit to experimental data; the coefficient κ accounts for the correlation between $M_{\rm bc}$ and ΔE.

To test and correct the shape of the background, we use events from the ΔE sidebands, which are defined as: $((\Delta E \pm 65\ {\rm MeV} + \kappa(M_{\rm bc} - m_B))/\sigma_{\Delta E})^2 + ((M_{\rm bc} - m_B)/\sigma_{M_{\rm bc}})^2 < 4$. Figure 4 shows the signal and sideband regions in the $M_{\rm bc}$-ΔE plane.

The $D\pi$ and $\pi\pi$ mass distributions for the signal events (sample 1) are shown in Fig. 5. In the $D\pi$ mass distribution a narrow peak corresponding to D^*_2 is evident. The $\pi\pi$ mass distribution shows a peak corresponding to the ρ meson as well as a structure at the 1.2–1.3 GeV/c^2 mass region that is presumably due to $f_0(1370)$ and $f_2(1270)$ production.

The $M^2_{D\pi}$ and $M^2_{\pi\pi}$ Dalitz plot distributions for the signal and sideband regions are shown in Fig. 6. The Dalitz plot boundary is fixed by the decay kinematics and the masses of the daughter particles. In order to have the same Dalitz plot boundary for both signal and sideband

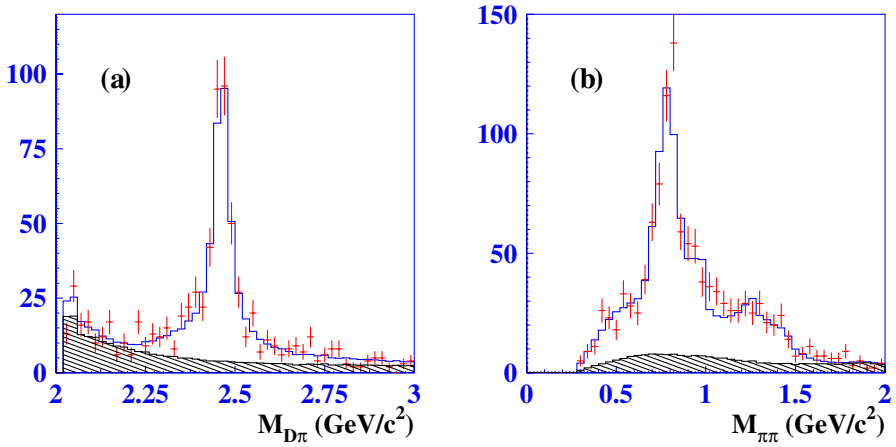

FIG. 5 (color online). $D\pi$ (a) and $\pi\pi$ (b) mass distributions for sample (1) events with corresponding ($\pi\pi$ or $D\pi$) helicity angles $\cos\theta_h > 0$. The points with error bars correspond to the signal region events, the hatched region indicates the background obtained from generic MC events normalized to the sideband data. The open histogram shows the fitted function after efficiency correction.

event samples, fits where the $K\pi$ mass is constrained to M_D and $D\pi\pi$ mass to m_B are performed. The mass-constrained fits also slightly improve the accuracy of $M^2_{D\pi}$ and $M^2_{\pi\pi}$.

To extract the amplitudes and phases of different intermediate states, an unbinned fit to the Dalitz plot is performed using the method described in Ref. [18]. The event density function in the Dalitz plot includes both the signal and background functions.

The backgrounds in the Dalitz plot are mostly combinatorial and have neither resonant structure [Fig. 6(b)] nor specific helicity behavior. The normalization and shape of the background in the signal region and delta E sideband is slightly different so we cannot use the sideband to get the background shape. To obtain the shape we use the generic MC which is separated into four components mentioned above. To improve consistency of data and MC we fit the data Dalitz plot in the sideband region to the sum of the MC contribution with the floating weights. After the weights are obtained we plot the MC Dalitz plot with these weights. The obtained distribution is parametrized by a smooth two-dimensional function which is used for the unbinned fit. The number of background events in the signal region is scaled according to the relative areas of the signal and sideband regions.

There is no general method to describe a three-body amplitude. In this paper we represent the $D\pi\pi$ amplitude as the sum of Breit-Wigner function contributions for different intermediate two-body states. Such an approach is not exact because it is neither analytic nor unitary and does not take into account a complete description of the final-state interactions. Nevertheless, the sum of Breit-Wigner functions describes the main features of the amplitude behavior and allows one to find and distinguish the contributions of two-body intermediate states, their interference, and the effective parameters of these states. We followed the same approach in the analysis of charged B decays [18].

In the $D^0\pi^+\pi^-$ final state, a combination of the D^0 meson and a pion can form a vector meson D^{*+}, a tensor

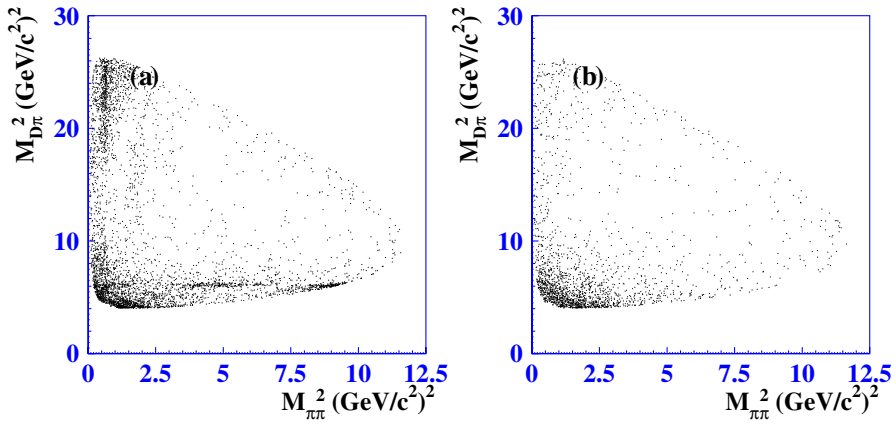

FIG. 6 (color online). The Dalitz plot for (a) signal events; (b) sideband events.

meson D_2^{*+}, or a scalar state D_0^{*+}; the axial vector mesons D_1^+ and $D_1'^+$ cannot decay to two pseudoscalars because of angular momentum and parity conservation. The region of $D^0\pi^+$ invariant mass that corresponds to the D^{*+} is excluded from the fit by requiring $|M_{D\pi} - M_{D^*}| > 3$ MeV/c^2. However, in B-meson decay, a virtual D^{*+} (referred to as D_v^*) can be produced off shell with $M_{D\pi}$ above the $D^0\pi^+$ production threshold and such a process can contribute to the amplitude. Another virtual hadron that can be produced in this combination is B^{*-} (referred to as B_v^*): $B \to B_v^*\pi$, and $B_v^* \to D\pi$. For the mass of B^{*-} as well as the mass and width of the D^{*+}, we use the PDG values [25]; the width of virtual B^{*-} is determined by weak processes and is taken equal to zero. To describe the $\pi\pi$ system we include ρ, ω, $f_2(1270)$, and three scalar mesons $f_0(600)$, $f_0(1370)$, and $f_0(980)$. The masses and widths of the ρ, ω, and $f_2(1270)$ mesons are fixed at their PDG values; the parameters of the scalar mesons are taken from the published papers on the $f_0(600)$ [28], $f_0(1370)$ [29], and $f_0(980)$ [29].

The contributions from the intermediate states listed above are included in the signal-event density ($S(q^2, q_1^2)$) parametrization as a coherent sum of the corresponding amplitudes together with a possible constant amplitude (a_{ps}). The phases of the amplitudes are defined relative to D_2^*:

$$\begin{aligned} S(q^2, q_1^2) = |&a_{D_2^*}A^{D_2^*}(q^2, q_1^2) + a_{D_0^*}e^{i\phi_{D_0^*}}A^{D_0^*}(q^2, q_1^2) \\ &+ a_{D_v^*}e^{i\phi_{D_v^*}}A^{D_v^*}(q^2, q_1^2) + a_\rho e^{i\phi_\rho}(A^\rho(q^2, q_1^2) \\ &+ r_{\omega-\rho}e^{i\phi_\omega}A^\omega(q^2, q_1^2)) \\ &+ a_{f_2}e^{i(\phi_{f_2}+\phi_\rho)}A^{f_2}(q^2, q_1^2) \\ &+ a_{f_0(600)}e^{i(\phi_{f_0(600)}+\phi_\rho)}A^{f_0(600)}(q^2, q_1^2) \\ &+ a_{f_0(980)}e^{i(\phi_{f_0(980)}+\phi_\rho)}A^{f_0(980)}(q^2, q_1^2) \\ &+ a_{f_0(1370)}e^{i(\phi_{f_0(1370)}+\phi_\rho)}A^{f_0(1370)}(q^2, q_1^2) \\ &+ a_{B_v^*}e^{i\phi_{B_v^*}}A^{B_v^*}(q^2, q_1^2) + a_{ps}e^{i\phi_{ps}}|^2, \end{aligned} \tag{1}$$

where $q^2 \equiv M_{D\pi}^2$ and $q_1^2 \equiv M_{\pi\pi}^2$, $\sum_i a_i^2 = 1$. The relative amplitude and phase of the ω meson are expressed via those of the ρ meson. The relative phase is taken from ρ-ω interference measurements [30], and the relative amplitude ($r_{\omega-\rho} = a_\omega/a_\rho$) is recalculated using that value. Assuming that the ρ and ω mesons produced in B^0 decay emerge from the $d\bar{d}$ pair, the relative amplitude is expected to satisfy a relation $r_{\omega-\rho(B)} = -3r_{\omega-\rho(\gamma)}$.

We use the approach described in [18], where each resonance is described by a relativistic Breit-Wigner function with a q^2 dependent width and an angular dependence that corresponds to the spin and parity of the intermediate- and final-state particles. The ρ meson amplitude is described by the Gounaris-Sakurai parametrization [31]. We take into account transition form factors for hadron transitions using the Blatt-Weisskopf parametrization [32] with a hadron scale $r = 1.6$ (GeV/c)$^{-1}$.

The variation of the detection efficiency over the Dalitz plot is taken into account by the minimization procedure. The efficiency dependence enters the likelihood function only through the normalization term. The normalization is obtained based on a large MC sample generated uniformly over the Dalitz plane, processed with the same selection criteria as the data and multiplied with the model used to fit the data. The detector resolution for the invariant mass of the $D\pi(\pi\pi)$ combination is about 2.5 (3.5) MeV/c^2, which is much smaller than the narrowest peak width of 30–40 MeV/c^2. Hence convolution of the described parametrization with the resolution is not necessary. The mass and width of the broad ($D\pi$) resonance, $M_{D_0^{*+}} = 2308$ MeV/c^2, $\Gamma^0_{D_0^{*+}} = 276$ MeV/c^2 are taken from our D^{**0} measurement [18].

Table II gives the fit results for different models. The contributions of different states are characterized by their fractions, which are defined as:

$$f_i = \frac{a_i^2 \int |A_i(Q)|^2 dQ}{\int |\sum_k a_k e^{i\phi_k} A_k(Q)|^2 dQ}, \tag{2}$$

where $A_i(Q)$ is the corresponding amplitude, and a_i and ϕ_i are the amplitude coefficients and phases obtained from the fit. The integration is performed over all available phase space characterized by the multidimensional vector Q (for decay to 3 spinless particles, $dQ \equiv dq^2 dq_1^2$), and i is one of the intermediate states: D_2^*, D_0^*, ρ, f_2, f_0, D_v^*, B_v^*, or the constant term a_{ps}. The sum of the individual fractions f_i may be different from unity because of interference. The product of the branching fractions of the B meson is expressed via the fraction f_i:

$$\mathcal{B}_{B\to i\pi}\mathcal{B}_{i\to D\pi} = \frac{N_{\rm sig} f_i}{N_{B\bar{B}}}, \tag{3}$$

where $N_{\rm sig}$ is the efficiency-corrected number of the reconstructed $D\pi\pi$ events and $N_{B\bar{B}}$ is the number of $B\bar{B}$ pairs produced.

Table II contains information on the likelihood change relative to the main set, and χ^2 values obtained as the sum of χ^2 for four histograms: projections of $M_{D\pi}$ and $M_{\pi\pi}$ for negative and positive helicities of the $D\pi$ and $\pi\pi$ systems, respectively [33]. χ^2's of two projections can be correlated so to determine a probability corresponding to χ^2 we perform toy MC generating the distribution on the Dalitz plot with a density corresponding to the experimental data and calculate χ^2. We used 1000 generated MC samples to determine the χ^2 distribution and list the probability values in the table.

The fit gives a statistically significant contribution from off-shell $D_v^*\pi$ production; the addition of the off-shell B_v^* amplitude does not improve the likelihood value significantly. The inclusion of the three-particle phase space term

TABLE II. The fit results for different sets of amplitudes. Option 1 is used as the main set of amplitudes for the final results. The presented errors are statistical only.

Options	1	2	3	4	5
States	D_2^*, D_0^*, D_v^*, ρ, f_2, $f_0's$	D_2^*, D_0^*, ρ, f_2, $f_0's$	D_2^*, D_0^*, D_v^*, ρ, f_2, $f_0's$, B_v^*	D_2^*, D_0^*, D_v^*, ρ, f_2, $f_0's + ps$	D_2^*, D_v^*, ρ, f_2, $f_0's$
$-2\ln\mathcal{L}/\mathcal{L}_0$	0	69.5	−2.7	−13.0	51.3
N_1	2181 ± 64	2174 ± 64	2223 ± 71	2264 ± 65	2111 ± 62
$\mathcal{B}_{B\to D_2^*\pi}\mathcal{B}_{D_2^*\to D\pi}(10^{-4})$	2.15 ± 0.16	2.23 ± 0.12	2.15 ± 0.18	2.26 ± 0.18	2.51 ± 0.14
$M_{D_2^*}$, (MeV/c^2)	2465.7 ± 1.8	2461.9 ± 1.6	2465.2 ± 1.9	2464.9 ± 1.6	2465.5 ± 1.7
$\Gamma_{D_2^*}$, (MeV/c^2)	49.7 ± 3.8	49.0 ± 3.9	49.3 ± 4.1	51.5 ± 3.8	55.4 ± 4.0
$\mathcal{B}_{B\to D_0^*\pi}\mathcal{B}_{D_0^*\to D\pi}(10^{-4})$	0.60 ± 0.13	0.61 ± 0.10	0.50 ± 0.13	0.79 ± 0.11	0
$\phi_{D_0^*}$	−3.00 ± 0.13	−2.28 ± 0.17	−2.88 ± 0.17	−2.66 ± 0.11	0
$M_{D_0^*}$, (MeV/c^2)	2308.0	2308.0	2308.0	2308.0	2308.0
$\Gamma_{D_0^*}$, (MeV/c^2)	276.0	276.0	276.0	276.0	276.0
$\mathcal{B}_{B\to D_v^*\pi}\mathcal{B}_{D_v^*\to D\pi}(10^{-4})$	0.88 ± 0.13	0	0.85 ± 0.14	0.74 ± 0.11	0.66 ± 0.10
$\phi_{D_v^*}$	−2.62 ± 0.15	0	−2.53 ± 0.17	−2.59 ± 0.13	−3.04 ± 0.20
$\mathcal{B}_{B\to D\rho}\mathcal{B}_{\rho\to\pi\pi}(10^{-4})$	3.19 ± 0.20	2.94 ± 0.15	3.15 ± 0.21	3.07 ± 0.14	3.26 ± 0.18
ϕ_ρ	2.25 ± 0.19	1.45 ± 0.22	1.81 ± 0.31	1.73 ± 0.15	1.89 ± 0.15
M_ρ, (MeV/c^2)	775.6	775.6	775.6	775.6	775.6
Γ_ρ, (MeV/c^2)	144.0	144.0	144.0	144.0	144.0
$\mathcal{B}_{B\to Df_2}\mathcal{B}_{f_2\to\pi\pi}(10^{-4})$	0.68 ± 0.10	0.64 ± 0.08	0.64 ± 0.09	0.54 ± 0.08	0.65 ± 0.08
ϕ_{f_2}	2.97 ± 0.21	2.48 ± 0.16	2.77 ± 0.20	2.32 ± 0.13	2.91 ± 0.17
M_{f_2}, (MeV/c^2)	1275.0	1275.0	1275.0	1275.0	1275.0
Γ_{f_2}, (MeV/c^2)	185.0	185.0	185.0	185.0	185.0
$\mathcal{B}_{B\to Df_0(600)}\mathcal{B}_{f_0(600)\to\pi\pi}(10^{-4})$	0.68 ± 0.08	0.72 ± 0.09	0.72 ± 0.09	0.47 ± 0.08	0.58 ± 0.07
$\phi_{f_0(600)}$	−0.44 ± 0.09	−0.42 ± 0.09	−0.40 ± 0.10	−0.43 ± 0.11	−0.32 ± 0.10
M_{f_0}, (MeV/c^2)	513.0	513.0	513.0	513.0	513.0
Γ_{f_0}, (MeV/c^2)	335.0	335.0	335.0	335.0	335.0
$\mathcal{B}_{B\to Df_0(980)}\mathcal{B}_{f_0(980)\to\pi\pi}(10^{-4})$	0.08 ± 0.04	0.11 ± 0.04	0.08 ± 0.04	0.04 ± 0.02	0.08 ± 0.03
$\phi_{f_0(980)}$	−2.48 ± 0.47	2.68 ± 0.37	−3.07 ± 0.51	2.87 ± 0.37	−2.85 ± 0.32
M_{f_0}, (MeV/c^2)	978.0	978.0	978.0	978.0	978.0
Γ_{f_0}, (MeV/c^2)	44.0	44.0	44.0	44.0	44.0
$\mathcal{B}_{B\to Df_0(1370)}\mathcal{B}_{f_0(1370)\to\pi\pi}(10^{-4})$	0.21 ± 0.10	0.24 ± 0.06	0.18 ± 0.06	0.15 ± 0.04	0.25 ± 0.10
$\phi_{f_0(1370)}$	−1.52 ± 0.56	3.08 ± 0.35	−2.43 ± 0.62	−2.75 ± 0.28	−2.00 ± 0.38
M_{f_0}, (MeV/c^2)	1434.0	1434.0	1434.0	1434.0	1434.0
Γ_{f_0}, (MeV/c^2)	173.0	173.0	173.0	173.0	173.0
$\mathcal{B}_{B\to B_v^*\pi}\mathcal{B}_{B_v^*\to D\pi}(10^{-4})$	0	0	0.74 ± 0.76	0	0
$\phi_{B_v^*}$	0	0	1.09 ± 0.51	0	0
ϕ_{ps}	0	0	0	0.22 ± 0.14	0
$\mathcal{B}_{ps}(10^{-4})$	0	0	0	0.33 ± 0.18	0
$\chi^2/N_{\rm dof}$	629/603	680/605	632/601	618/601	659/605
C.L. (%)	32	10	29	34	17

improves the likelihood value, however there is no reason to expect a constant amplitude with no momentum dependence over such a wide range of final particle momenta. Table III shows that the likelihood changes significantly when the broad resonance D_0^* is removed or treated as either a vector or a tensor. The change of likelihood $-2\ln\mathcal{L}/\mathcal{L}_0 = 51$ for 2 additional degrees of freedom (amplitude and phase of D_0^*) corresponds to a significance of 6.8σ [34]. The significance is calculated based on the $\ln\mathcal{L}$ difference.

TABLE III. Changes in likelihood for different quantum number assignments for the broad resonance.

	No broad state	0^+	1^-	2^+
$-2\ln\mathcal{L}/\mathcal{L}_0$	51	0	28	27
$\chi^2/N_{\rm dof}$	659/605	629/603	652/603	640/603
C.L. (%)	16	32	19	25

The branching fractions of D_2^* and D_0^* remain constant within errors for different models. The set of states used for the final results are D_2^*, D_0^*, D_v^*, ρ, f_2 and the three above-listed f_0's, corresponding to column 1 in Table II.

The values of the D_2^{*+} resonance mass and width obtained from the fit are:

$$M_{D_2^{*+}} = (2465.7 \pm 1.8 \pm 0.8^{+1.2}_{-4.7})\ \mathrm{MeV}/c^2,$$
$$\Gamma_{D_2^{*+}} = (49.7 \pm 3.8 \pm 4.1 \pm 4.9)\ \mathrm{MeV},$$

where the third error is model uncertainty. These parameters are consistent with but more precise than previous measurements performed by CLEO $M_{D_2^{*0}} = (2463 \pm 3 \pm 3)\ \mathrm{MeV}/c^2$ [8] and FOCUS $\Gamma_{D_2^*} = (34.1 \pm 6.5 \pm 4.2)$ MeV [35].

The product of the branching fraction for D_2^* production obtained from the fit is:

$$\mathcal{B}(\bar{B}^0 \to D_2^{*+}\pi^-) \times \mathcal{B}(D_2^{*+} \to D^0\pi^+) = (2.15 \pm 0.17 \pm 0.29 \pm 0.12) \times 10^{-4},$$

where the three errors are statistical, systematic, and a model-dependent error, respectively. We observe the production of the broad scalar D_0^{*+} state with the product branching fraction,

$$\mathcal{B}(\bar{B}^0 \to D_0^{*+}\pi^-) \times \mathcal{B}(D_0^{*+} \to D^0\pi^+) = (0.60 \pm 0.13 \pm 0.15 \pm 0.22) \times 10^{-4}.$$

This is the first observation of this decay (the interpretation of the neutral partner of this state is still a subject of theoretical discussion [36]). The relative phase of the D_0^* amplitude is

$$\phi_0 = 3.00 \pm 0.13 \pm 0.10 \pm 0.43.$$

The $D\pi$ helicity angle distributions for $M_{D\pi}$ regions corresponding to the D_2^* and D_0^* are shown in Fig. 7(a) and 7(b), respectively, together with the efficiency-corrected fitting function. The histogram in the region of the D_2^* meson clearly indicates a D wave. The distributions in the other regions show reasonable agreement between the fitting function and the data.

The uncertainty of the background is one of the main sources of systematic error. It is estimated by comparing the fit results of the default fit, the fit where the weights of the individual four background categories are set to unity, and fit where only upper or lower ΔE sideband was used to obtain the background shape. The fit is also performed with more restrictive and looser cuts on ΔE, M_{bc}, and M_D that change the signal-to-noise ratio by factors of about two. The results obtained are consistent with each other and the maximum difference is taken as an additional estimate of the systematic uncertainty. The systematic errors on the $\mathcal{B}_i$ measurements (Eq. (3)) for the individual intermediate states include uncertainties in track reconstruction and particle identification efficiency, as well as the error in the $D^0 \to K^-\pi^+$ absolute branching fraction. The model uncertainties are estimated by comparing fit results for the case of different models and for values of the parameter r of the transition form factor [32] from 0 to 3 $(\mathrm{GeV}/c)^{-1}$.

The $\pi\pi$ helicity angle distributions for $M_{\pi\pi}$ ranges corresponding to the ρ, f_2 and the region below the ρ, where the broad resonance dominates, are shown in Fig. 8. For the positive helicity region, where the $D\pi$ contribution is suppressed, a clear P-wave structure for the ρ and D-wave structure for the f_2 is observed. The scalar component parameters cannot be determined from the fit. This process can also have contributions from nonresonant background. The product branching fraction for the f_2 is

$$\mathcal{B}(\bar{B}^0 \to D^0 f_2)\mathcal{B}(f_2 \to \pi^+\pi^-) = (0.68 \pm 0.10 \pm 0.12 \pm 0.18) \times 10^{-4}.$$

Taking into account the branching fraction $\mathcal{B}(f_2 \to \pi\pi) = 0.847^{+0.025}_{-0.012}$ [25] and the corresponding Clebsch-Gordan coefficients, we obtain

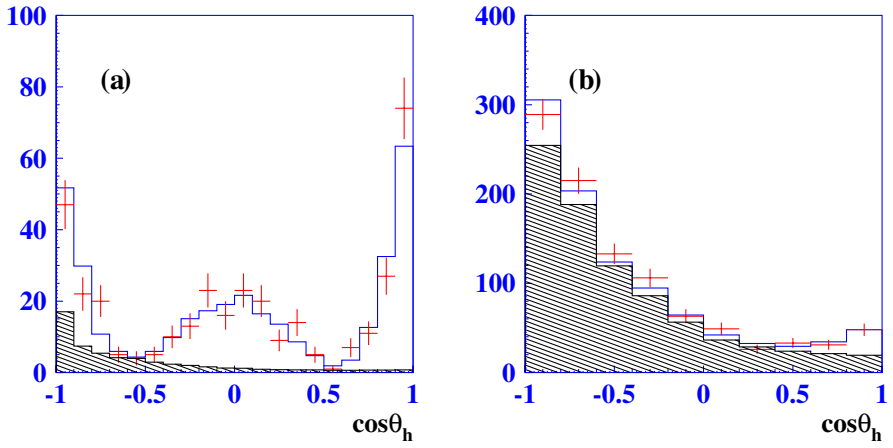

FIG. 7 (color online). $D\pi$ helicity angle distributions for data (points) and MC (histogram). The hatched distribution shows the background from the ΔE sideband region with the appropriate normalization. (a) corresponds to the D_2^* region $|M_{D\pi} - 2.46| < 0.1\ \mathrm{GeV}/c^2$; (b) the D_0^* region $|M_{D\pi} - 2.30| < 0.1\ \mathrm{GeV}/c^2$.

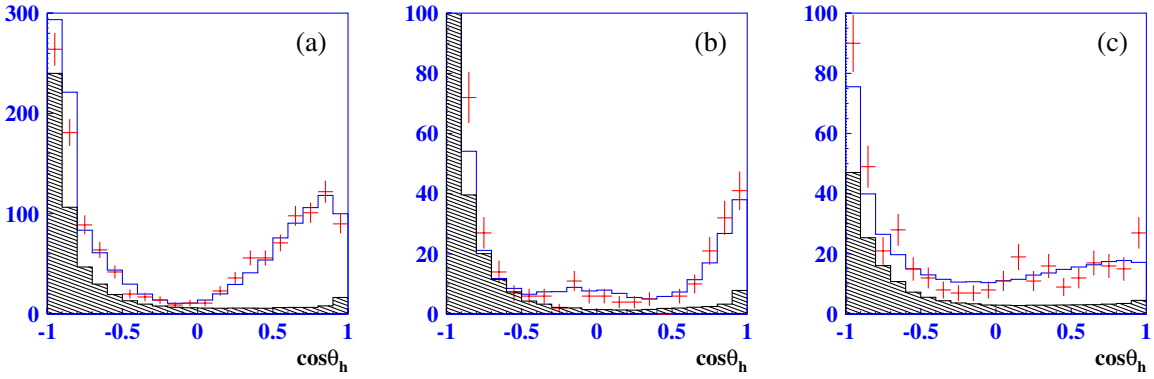

FIG. 8 (color online). $\pi\pi$ helicity angle distributions for data (points) and MC (histogram). The hatched distribution shows the background distribution from the ΔE sideband region with appropriate normalization. (a) corresponds to the ρ region $|M_{\pi\pi} - 0.78| < 0.2$ GeV/c^2; (b) the f_2 region $|M_{\pi\pi} - 1.20| < 0.1$ GeV/c^2; (c) the f_0 region $M_{\pi\pi} < 0.60$ GeV/c^2.

$$\mathcal{B}(\bar{B}^0 \to D^0 f_2) = (1.20 \pm 0.18 \pm 0.21 \pm 0.32) \times 10^{-4},$$
$$\mathcal{B}(\bar{B}^0 \to D^0 \rho^0) = (3.19 \pm 0.20 \pm 0.24 \pm 0.38) \times 10^{-4}.$$

The phases relative to the D_2^* amplitude are $\phi_\rho = 2.25 \pm 0.19 \pm 0.20^{+0.21}_{-0.99}$ and $\phi_{f_2} = 2.97 \pm 0.21 \pm 0.13 \pm 0.45$.

B. Results and discussion

The branching fraction products obtained for the narrow ($j = 3/2$) resonances are similar to the published results for charged B decays as shown in Table IV. The measured values of the branching fractions for the broad D_0^{*+} resonances in neutral B decays are, however, significantly lower than those for charged B decays. Preliminary data on $\bar{B}^0 \to D^{*0}\pi^+\pi^-$ decay [19] shown in Table IV indicates a similar behavior for $D_1'^0$ and D_1^0 production. One possible explanation for this phenomenon is that for charged B decay to $D^{**}\pi$, the amplitude receives contributions from both tree and color-suppressed diagrams as shown in Fig. 2. For the color-suppressed diagrams, however, D^{**}'s are produced by another mechanism and the amplitudes are characterized by the decay constants $f_{D(3/2)}$ and $f_{D(1/2)}$, with $f_{D(3/2)} \ll f_{D(1/2)}$. The production of the broad resonances D_0^{*0} and $D_1'^0$ in charged B decay is amplified by the color-suppressed amplitude. As shown in [37], in such a case both $\tau_{1/2}$ fits to the sum rule and the value of $f_{D(1/2)}$ are consistent with theoretical estimates.

V. CONCLUSION

A study of neutral B-meson decays to $D^0\pi^+\pi^-$ is reported. We measure the total branching fraction of the three-body $D^0\pi^+\pi^-$ decays, obtaining $\mathcal{B}(\bar{B}^0 \to D^0\pi^+\pi^-) = (8.4 \pm 0.4 \pm 0.8) \times 10^{-4}$. The intermediate resonant structure of these three-body decays is studied. The $D^0\pi^+\pi^-$ final state is described by the production of $D_{0,2}^*\pi^-$ with subsequent decays $D_{0,2}^* \to D\pi$, and also by $D\rho$, Df_2, and Df_0, where f_0 is a broad scalar ($\pi\pi$) structure. From a Dalitz plot analysis we obtain the mass, width, and product of the branching fractions for the D_2^{*+}:

$$M_{D_2^{*+}} = (2465.7 \pm 1.8 \pm 0.8^{+1.2}_{-4.7}) \text{ MeV}/c^2,$$
$$\Gamma_{D_2^{*+}} = (49.7 \pm 3.8 \pm 4.1 \pm 4.9) \text{ MeV},$$
$$\mathcal{B}(\bar{B}^0 \to D_2^{*+}\pi^-) \times \mathcal{B}(D_2^{*+} \to D^0\pi^+) = (2.15 \pm 0.17 \pm 0.29 \pm 0.12) \times 10^{-4}.$$

We observe the production of the broad scalar D_0^{*+} state with the product branching fraction

$$\mathcal{B}(\bar{B}^0 \to D_0^{*+}\pi^-) \times \mathcal{B}(D_0^{*+} \to D^0\pi^+) = (0.60 \pm 0.13 \pm 0.15 \pm 0.22) \times 10^{-4}.$$

This is the first observation of this decay. The phase of the D_0^* amplitude relative to that of the D_2^* is determined to be:

$$\phi_0 = 3.00 \pm 0.13 \pm 0.10 \pm 0.43.$$

The $B \to D\rho$ and Df_2 branching fractions are measured to be:

TABLE IV. Comparison of product branching fractions for neutral and charged B decays.

	Neutral B	Charged B [18]
$\mathcal{B}(\bar{B} \to D_2^*\pi^-)\mathcal{B}(D_2^* \to D\pi)$	$(2.15 \pm 0.17 \pm 0.29 \pm 0.12) \times 10^{-4}$	$(3.4 \pm 0.3 \pm 0.6 \pm 0.4) \times 10^{-4}$
$\mathcal{B}(\bar{B} \to D_2^*\pi^-)\mathcal{B}(D_2^* \to D^*\pi)$	$(2.45 \pm 0.42^{+0.35+0.39}_{-0.45-0.17}) \times 10^{-4}$ [19]	$(1.8 \pm 0.3 \pm 0.3 \pm 0.2) \times 10^{-4}$
$\mathcal{B}(\bar{B} \to D_1\pi^-)\mathcal{B}(D_1 \to D^*\pi)$	$(3.68 \pm 0.60^{+0.71+0.65}_{-0.40-0.30}) \times 10^{-4}$ [19]	$(6.8 \pm 0.7 \pm 1.3 \pm 0.3) \times 10^{-4}$
$\mathcal{B}(\bar{B} \to D_0^*\pi)\mathcal{B}(D_0^* \to D\pi)$	$(0.60 \pm 0.13 \pm 0.15 \pm 0.22) \times 10^{-4}$	$(6.1 \pm 0.6 \pm 0.9 \pm 1.6) \times 10^{-4}$
$\mathcal{B}(\bar{B} \to D_1'\pi^-)\mathcal{B}(D_1' \to D^*\pi)$	$<0.7 \times 10^{-4}$ at 90% C.L. [19]	$(5.0 \pm 0.4 \pm 1.0 \pm 0.4) \times 10^{-4}$

$$\mathcal{B}(\bar{B}^0 \to D^0\rho^0) = (3.19 \pm 0.20 \pm 0.24 \pm 0.38) \times 10^{-4},$$

$$\mathcal{B}(\bar{B}^0 \to D^0 f_2) = (1.20 \pm 0.18 \pm 0.21 \pm 0.32) \times 10^{-4},$$

and the phases relative to the D_2^* amplitude are:

$$\phi_\rho = 2.25 \pm 0.19 \pm 0.20^{+0.21}_{-0.99},$$

$$\phi_{f_2} = 2.97 \pm 0.21 \pm 0.13 \pm 0.45.$$

This is the first observation of the $\bar{B}^0 \to D^0 f_2$ decay.

ACKNOWLEDGMENTS

We thank the KEKB group for the excellent operation of the accelerator, the KEK Cryogenics group for the efficient operation of the solenoid, and the KEK computer group and the National Institute of Informatics for valuable computing and Super-SINET network support. We acknowledge support from the Ministry of Education, Culture, Sports, Science, and Technology of Japan and the Japan Society for the Promotion of Science; the Australian Research Council and the Australian Department of Education, Science and Training; the National Science Foundation of China under Contract No. 10175071; the Department of Science and Technology of India; the BK21 program of the Ministry of Education of Korea and the CHEP SRC program of the Korea Science and Engineering Foundation; the Polish State Committee for Scientific Research under Contract No. 2P03B 01324; the Ministry of Science and Technology of the Russian Federation; the Ministry of Education, Science and Sport of the Republic of Slovenia; the National Science Council and the Ministry of Education of Taiwan; and the U.S. Department of Energy.

[1] H. Albrecht *et al.* (ARGUS Collaboration), Phys. Rev. Lett. **56**, 549 (1986).
[2] H. Albrecht *et al.* (ARGUS Collaboration), Phys. Lett. B **221**, 422 (1989).
[3] H. Albrecht *et al.* (ARGUS Collaboration), Phys. Lett. B **232**, 398 (1989).
[4] J. C. Anjos *et al.* (Tagged Photon Spectrometer Collaboration), Phys. Rev. Lett. **62**, 1717 (1989).
[5] P. Avery *et al.* (CLEO Collaboration), Phys. Rev. D **41**, 774 (1990).
[6] P. L. Frabetti *et al.* (E687 Collaboration), Phys. Rev. Lett. **72**, 324 (1994).
[7] P. Avery *et al.* (CLEO Collaboration), Phys. Lett. B **331**, 236 (1994); **342**, 453(E) (1995).
[8] T. Bergfeld *et al.* (CLEO Collaboration), Phys. Lett. B **340**, 194 (1994).
[9] D. Bloch *et al.* (DELPHI Collaboration), Report Nos. CERN-OPEN-2000-015, DELPHI-98-128-CONF-189, 1998, p. 12.
[10] D. Bloch *et al.* (DELPHI Collaboration), Report No. DELPHI-2000-106-CONF 405.
[11] D. Buskulic *et al.* (ALEPH Collaboration), Z. Phys. C **73**, 601 (1997).
[12] N. Isgur and M. B. Wise, Phys. Rev. Lett. **66**, 1130 (1991).
[13] J. L. Rosner, Comments Nucl. Part. Phys. **16**, 109 (1986).
[14] S. Godfrey and R. Kokoski, Phys. Rev. D **43**, 1679 (1991).
[15] A. F. Falk and M. E. Peskin, Report No. SLAC-PUB-6311, 1993.
[16] N. Uraltsev, Phys. Lett. B **501**, 86 (2001).
[17] A. Le Yaouanc *et al.*, Phys. Lett. B **520**, 25 (2001).
[18] K. Abe *et al.* (Belle Collaboration), Phys. Rev. D **69**, 112002 (2004).
[19] K. Abe *et al.* (Belle Collaboration), arXiv:hep-ex/0412072.
[20] A. Abashian *et al.* (Belle Collaboration), Nucl. Instrum. Methods Phys. Res., Sect. A **479**, 117 (2002).
[21] Events are generated with a modified version of the CLEO group's QQ program (http://www.lns.cornell.edu/public/CLEO/soft/QQ); the detector response is simulated using GEANT, R. Brun *et al.*, GEANT 3.21, CERN Report No. DD/EE/84-1, 1984.
[22] E. Nakano, Nucl. Instrum. Methods Phys. Res., Sect. A **494**, 402 (2002).
[23] The z coordinate of the track is defined as the z coordinate of the track point closest to the beam in the r-ϕ plane. The z axis is opposite to the positron beam direction.
[24] We use $D^0\pi^+$ and $\bar{D}^0\pi^-$ for $\bar{B}^0$ and B^0 decays, respectively.
[25] W.-M. Yao *et al.* (Particle Data Group), J. Phys. G **33**, 1 (2006).
[26] A. Satpathy *et al.* (Belle Collaboration), Phys. Lett. B **553**, 159 (2003).
[27] G. Brandenburg *et al.* (CLEO Collaboration), Phys. Rev. Lett. **80**, 2762 (1998).
[28] H. Muramatsu *et al.*, Phys. Rev. Lett. **89**, 251802 (2002).
[29] E. M. Aitala *et al.*, Phys. Rev. Lett. **86**, 765 (2001).
[30] R. R. Akhmetshin *et al.* (CMD-2 Collaboration), Phys. Lett. B **527**, 161 (2002).
[31] G. J. Gounaris and J. J. Sakurai, Phys. Rev. Lett. **21**, 244 (1968).
[32] J. Blatt and V. Weisskopf, *Theoretical Nuclear Physics* (John Wiley & Sons, New York, 1952), p. 361.
[33] The overall χ^2 is calculated as the sum of the χ^2's from four distributions: two 160-bin histograms of $M_{D\pi}$ for positive and negative helicities of the $D\pi$ system, and two 150-bin histograms $M_{\pi\pi}$ with positive and negative helicities of the $\pi\pi$ system. The number of degrees of freedom is calculated as the number of bins minus the number of free parameters.
[34] S. S. Wilks, Ann. Math. Stat. **9**, 60 (1938).
[35] J. M. Link *et al.* (FOCUS Collaboration), Phys. Lett. B **586**, 11 (2004).
[36] M. E. Bracco, A. Lozea, R. D. Matheus, F. S. Navarra, and M. Nielsen, Phys. Lett. B **624**, 217 (2005).
[37] F. Jugeau, A. Le Yaouanc, L. Oliver, and J. C. Raynal, Phys. Rev. D **72**, 094010 (2005).